Spatio-temporal hybrid color-polarization channeled sensors

Israel J. Vaughn[a] and J. Scott Tyo[a]

[a]University of New South Wales Canberra, ACT, Australia

ABSTRACT

Recent advancements in channeled spatio-temporal polarization sensor systems have shown potential for improved imaging performance. Lithographic processes now allow for the manufacture of pixelated focal plane arrays with both color and polarization filters applied at the per pixel level. Both Sony and Pau's group at the University of Arizona have demonstrated the manufacture of these hybrid sensors. These new sensors produce spatially channeled hybrid color/polarization systems and crowd the available channel bandwidth space in the Nyquist square. We present a new system design which utilises polarization elements to generate additional temporal carriers, allowing for the separation of color and polarization channels. This separation has the potential to improve the hybrid system performance for certain classes of scene statistics and is analogous to a kind of super-resolution effect similar to a vibrating sensor or using motion for subsampling. The separation can be achieved by varying the polarization sensitive pixels in time, e.g. a rotating half waveplate or an electro-optic polarization element. We show the system design for an existing COTS Sony sensor as well as a design with improved performance over the Sony focal plane array, along with preliminary results on possible system performance.

Keywords: polarimetry, modulated polarimetry, linear systems, microanalyzer array, micropolarizer array, polarimetric channels, color-polarimetric hybrid

1. INTRODUCTION

Passive polarimetric instruments can be viewed via a communications theory framework, where the measurement of polarimetric information can be described via carriers and channels. If the carriers are sinusoids, then the channels are delta functions, and if there is sampling then the channels become sinc functions.[1,2] Carriers of

Send correspondence to IJV
IJV: israel.vaughn@gmail.com

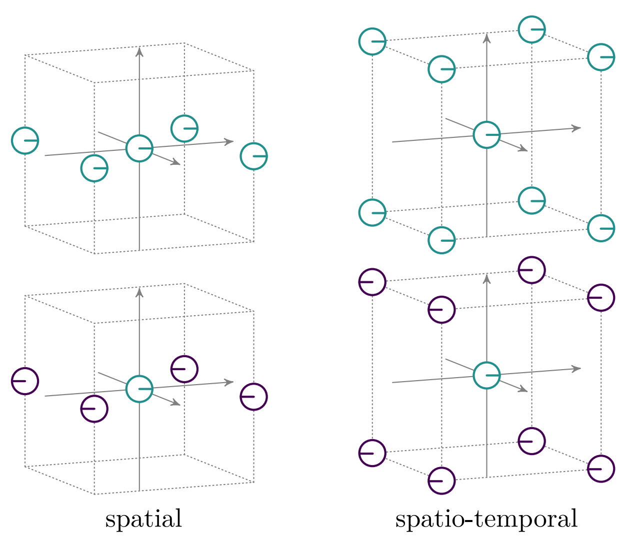

Figure 1: Spatio-temporal example showing the Nyquist cube in the spatio-temporal frequency space. Left shows spatial only channels, right shows spatio-temporal channels. The axes are (ξ, η, ν) and range from -0.5 to 0.5 in arbitrary frequency units.

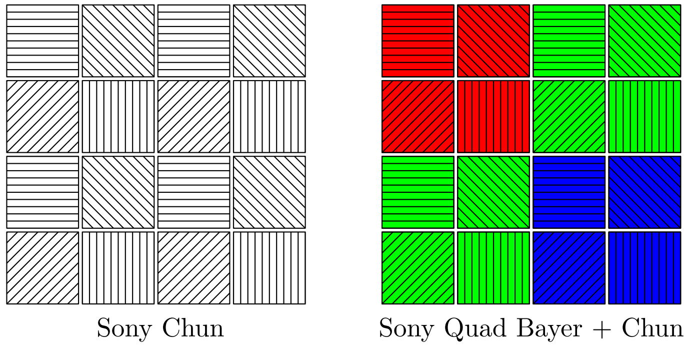

Figure 2: Micropolarizer layout of typical Chun unit cells for micropolarizer array sensors (left). The new Sony color hybrid sensor, using a Chun unit cell for the micropolarizer layout (right).

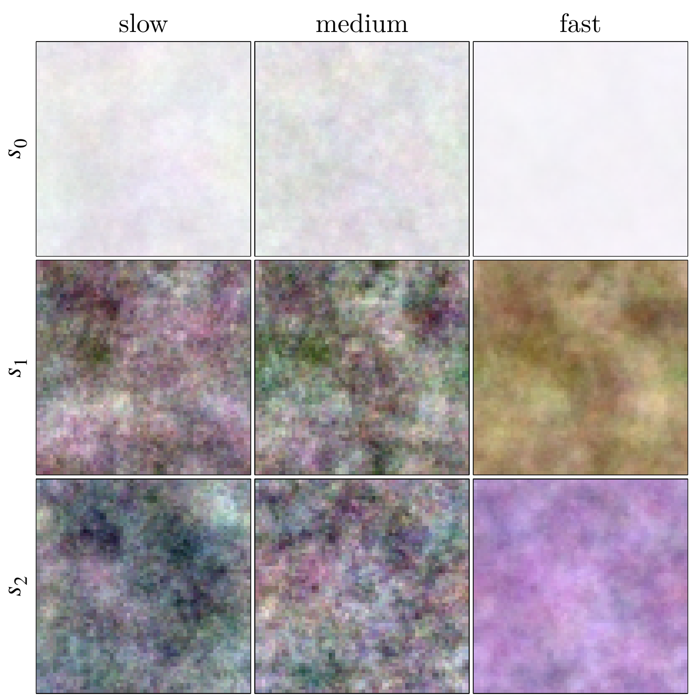

Figure 3: Input data (click figure picture for animation) for slow, medium, and fast temporal bandwidths. Modeled for a mean of about 3000 photo electrons, and assuming a 12-bit sensor depth. The red, blue, green color coding for s_0 is directly proportional to the actual input values. The red, green, and blue coding for s_1, s_2 have been rescaled and normalized to fit in $[0, 255]$ for each color since there are no negative values in the RGB display values. Each data cube input is $64 \times 64 \times 64$ in x-pixels, y-pixels, and frames respectively for the 9 color-polarimetric parameters.

.

polarimetric information can be generated via a number of methods.[2–4] The general irradiance for a Stokes polarimeter can be described by the following equation:

$$\begin{aligned} s_{0,\mathrm{out}}(\mathbf{x}) = a_0(\mathbf{x}) \cdot s_{0,\mathrm{obj}}(\mathbf{x}) + a_1(\mathbf{x}) \cdot s_{1,\mathrm{obj}}(\mathbf{x}) \\ + a_2(\mathbf{x}) \cdot s_{2,\mathrm{obj}}(\mathbf{x}) + a_3(\mathbf{x}) \cdot s_{3,\mathrm{obj}}(\mathbf{x}). \end{aligned} \tag{1}$$

The parameter set $\mathbf{x}$ represents a set of independent variables such as space,[1,2,5,6] time,[3,7,8] wavelength,[9] angle of incidence,[10] etc., and the functions $a_0(\mathbf{x}) - a_3(\mathbf{x})$ generate the carriers. Real instruments take discrete measurements. If $\mathbf{A}(\mathbf{x})$ is known, then the right hand side (RHS) of Equation (1) can be rewritten as

$$\begin{bmatrix} a_{00}(\mathbf{x}_j) & a_{01}(\mathbf{x}_j) & a_{02}(\mathbf{x}_j) & a_{03}(\mathbf{x}_j) \end{bmatrix} \cdot \begin{bmatrix} s_{0,\mathrm{obj}}(\mathbf{x}_j) \\ s_{1,\mathrm{obj}}(\mathbf{x}_j) \\ s_{2,\mathrm{obj}}(\mathbf{x}_j) \\ s_{3,\mathrm{obj}}(\mathbf{x}_j) \end{bmatrix} \tag{2}$$

for each $\mathbf{x}_j$. The system of equations is then:

$$\mathbf{g}_{s_{0,\mathrm{out}}} = \begin{bmatrix} a_0(\mathbf{x}_0) & a_1(\mathbf{x}_0) & a_2(\mathbf{x}_0) & a_3(\mathbf{x}_0) \\ a_0(\mathbf{x}_1) & a_1(\mathbf{x}_1) & a_2(\mathbf{x}_1) & a_3(\mathbf{x}_1) \\ \vdots & \vdots & \vdots & \vdots \\ a_{00}(\mathbf{x}_{n-1}) & a_{01}(\mathbf{x}_{n-1}) & a_{02}(\mathbf{x}_{n-1}) & a_{03}(\mathbf{x}_{n-1}) \end{bmatrix} \cdot \begin{bmatrix} s_{0,\mathrm{obj}}(\mathbf{x}_{\lfloor (n-1)/2 \rceil}) \\ s_{1,\mathrm{obj}}(\mathbf{x}_{\lfloor (n-1)/2 \rceil}) \\ s_{2,\mathrm{obj}}(\mathbf{x}_{\lfloor (n-1)/2 \rceil}) \\ s_{3,\mathrm{obj}}(\mathbf{x}_{\lfloor (n-1)/2 \rceil}) \end{bmatrix} = \mathbf{W} \cdot \mathbf{s} \tag{3}$$

These equations require assumptions that we have discussed in past literature.[11,12] An equivalent expression for Eq. (1) is in the Fourier, or channel domain:

$$S_{0,\mathrm{out}}(\boldsymbol{\rho}) = \sum_{j=0}^{3} A_j(\boldsymbol{\rho}) * \mathbf{S}_j(\boldsymbol{\rho}) \tag{4}$$

where $*$ denotes convolution, $\mathbf{x} \rightarrow \boldsymbol{\rho}$ are the Fourier dual variables, A_j are the Fourier transforms of the analyzer functions, and S_j are the Fourier transforms of the Stokes object functions. In this article we use the spatio-temporal domain (x, y, t), and the Fourier dual (ξ, η, ν). When the functions a_{mn} are periodic in $\mathbf{x}$, then their Fourier transforms A_{mn} create a grid of δ-functions in $\boldsymbol{\rho}$. We denote the set of δ-functions the system's *channels*.

2. SPATIO-TEMPORAL CHANNELS

Prior work by our group[1,2,5,7,8,11–14] and others[2,4] have explored spatially and spatio-temporally channeled Stokes polarimeters.[2,4] However, no analysis that we know of for hybrid color and polarization sensors as channeled imaging systems has been done. Hybrid polarization and color micro-patterned sensors were first produced by Pau's group.[15] Recently, Sony began manufacturing and selling a hybrid color and polarization hybrid micro-patterned focal plane array, the IMX250MYR.[16] For this category of system, we can rotate (or otherwise temporally vary) the micropolarizers by using a half-wave retarder. In this article we present preliminary analysis of these color-polarization hybrid systems as spatio-temporal channeled systems, and make the case that Sony should have used the dual tiling of what they manufactured as prototyped by Tu *et al.*[15]

Spatio-temporal channels reside in a 3-dimensional frequency space and provide more degrees of freedom for imaging system design. All channel structure plots in this article are normalized to arbitrary frequency units in the Nyquist square or Nyquist cube since we assume sampling in our imaging systems. Figure 1 shows spatio-temporal channels versus spatial channels. The circles denote the location of the channels (δ-functions), the area of the circle is proportional to the magnitude, and the clocking and color represent the complex value, i.e., a circle with the clock hand pointing right is purely real and positive, left is purely real and negative, up is purely imaginary and positive, down is purely imaginary and negative.

Spatial and spatio-temporal channel structures have been well defined in the current literature,[2,4,5,12,13] but we briefly review them here. Periodic structures on a focal plane, as shown in Figure 2, generate channels in spatial frequency space. The spatial channel structure of the panchromatic Chun pattern has been produced

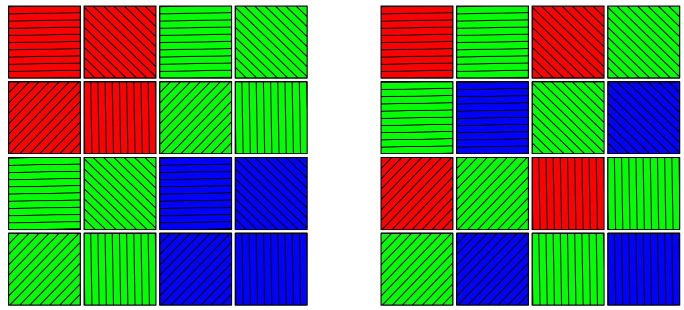

Figure 4: Layout of the new Sony color hybrid sensor (left). Tu's layout (right). Click figure picture for animation.

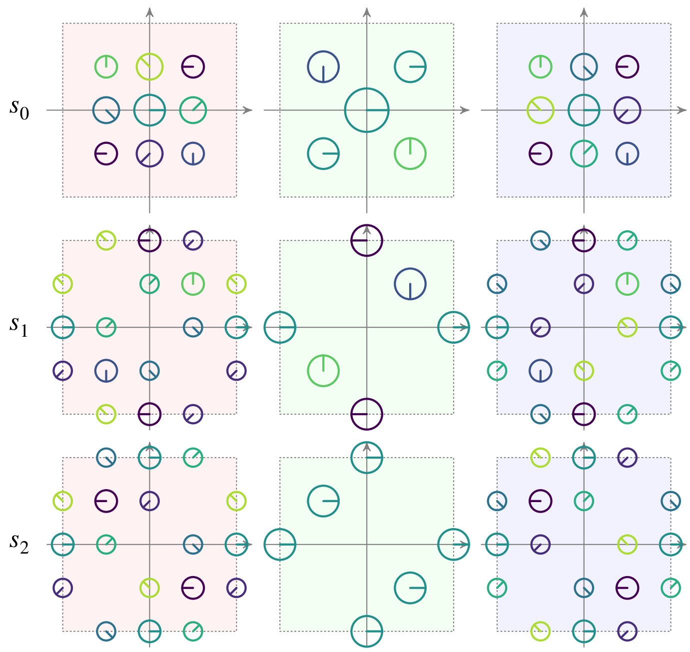

Figure 5: Spatial channel structure of the new Sony hybrid sensor, s_0 is shown in the first row, s_1 in the second row, and s_2 in third row. The first column is red, the second is green, and the third is blue.

elsewhere[4,5] so we don't reproduce it here. When a half wave plate is rotated in front of the Chun pattern, a spatio-temporal channel structure is generated.[12,13] Analogously, a spatio-temporal hybrid channel structure can also be generated from the color-polarization hybrid sensor shown in Figure 2 by rotating a half waveplate in front of the focal plane array. There are a number of choices for a micropatterned hybrid sensor, including triband color filters and a number of arrangements for the polarization filters. We introduce a preliminary analysis here assuming typical glass color micropatterned filters without mixed spectral bandpasses, i.e. each color filter passes only red, only green, or only blue. We also assume linear micropolarizers and half wave retardance rotation at the global level, i.e. uniformly across the sensor plane.

If polarization measurements are taken at each color then the total number of parameters that can be measured are 9, $s_{r,0}$, $s_{r,1}$, $s_{r,2}$, $s_{g,0}$, $s_{g,1}$, $s_{g,2}$, $s_{b,0}$, $s_{b,1}$, $s_{b,2}$ where r, g, b denote red, green, and blue respectively. In the analysis we model the imaging of the systems using spatio-temporal data sampled from a statistical power law distribution[17] which approximates natural scenes (with no horizon). This data allows comparison of reconstruction performance between the systems to be discussed. An example frame of the input data is shown in Figure 3.

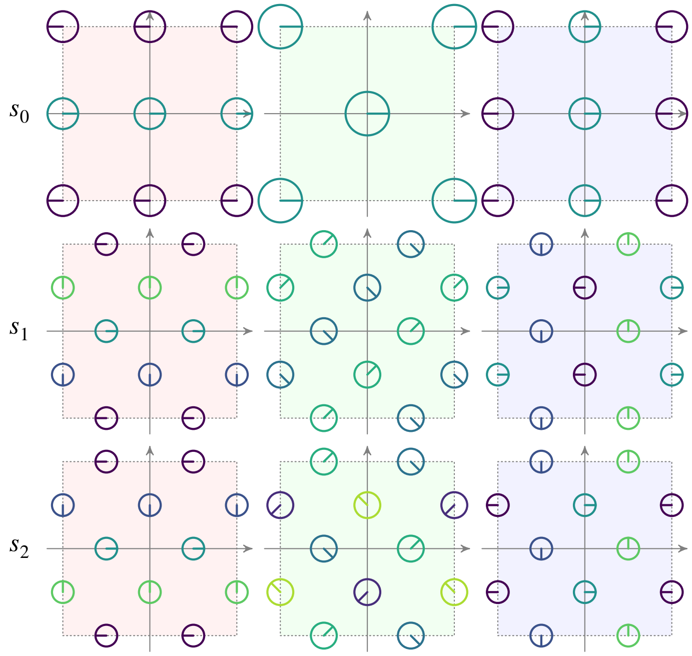

Figure 6: Spatial channel structure of the Tu hybrid layout, s_0 is shown in the first row, s_1 in the second row, and s_2 in third row. The first column is red, the second is green, and the third is blue.

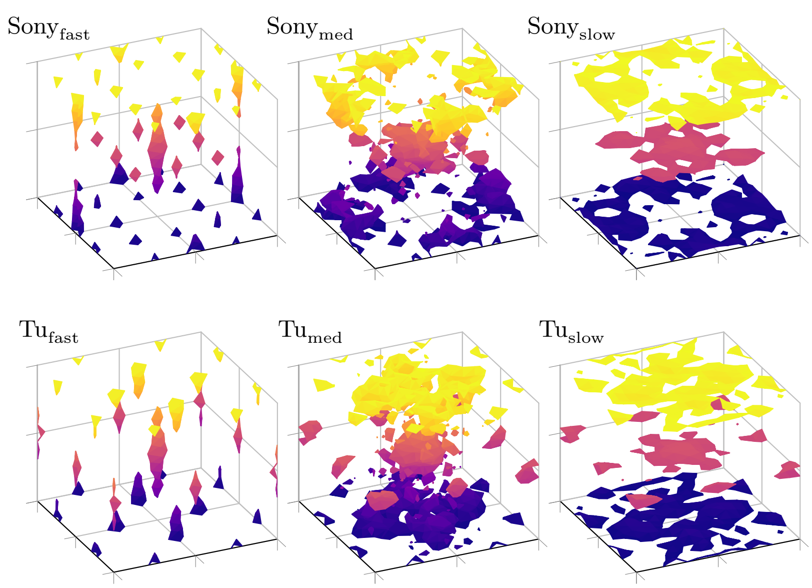

Figure 7: Isosurfaces of Fourier transform magnitudes: top row for the Sony layout, bottom row for the Tu layout. Subscripts denote bandwidth scenarios: (fast) low spatial, high temporal, (med) medium spatial, medium temporal, (slow) high spatial, low temporal. To aid depth perception, data is colored in accordance with its position along the temporal frequency axis that is mapped into the Cartesian z. Note that the Stokes data is positioned within the Nyquist-cube, and the input data cube is identical for both systems.

3. HYBRID SENSORS

Tu *et al* in Stanley Pau's group at the University of Arizona built a color hybrid sensor using a pattern (Figure 4 right) different from the one that Sony produced (Figure 4 left). The Tu pattern uses larger micropolarizers, i.e. a single micropolarizer covers a typical Bayer pattern unit cell; four Bayer unit cells (for 16 total pixels) are tiled in the Chun pattern by the polarizers. Sony uses a "quad Bayer" pattern which they recently introduced for low light imaging into cell phone sensors. The quad Bayer has 2×2 blocks of a single color, and each of the single color blocks is covered by a Chun polarizer pattern. The spatial only channel structure for the Sony implementation is shown in Figure 5. Note that the channel space is quite crowded. When a half wave retarder is rotated in front of the sensor, the s_0 channels will remain in the temporal $\nu = 0$ frequency plane, while the s_1, s_2 channels will be split to the faces of the Nyquist cube at $\nu = \pm 0.5$. The spatial only channel structure for the Tu layout is shown in Figure 6. The packing of the channels for the Tu layout is lower density, corresponding to increased spatial bandwidth potential. When the s_1, s_2 channels are split in the ν direction by addition of the half wave retarder, they are offset spatially from the s_0 channels which remain in the $\nu = 0$ frequency plane, reducing channel crosstalk. Even for a spatial only imager the Tu pattern channel structure has more bandwidth available between channels.

To characterize the performance of the Tu and Sony systems, we generate random sets of representative spatio–temporal colored linear Stokes data, pass them through a forward instrument model, reconstruct the data cubes, and finally compute the peak signal-to-noise ratio (PSNR) of the reconstructed data. As in previous work, we use a forward model that uses only Mueller calculus at each pixel with the assumption that the spectral filters are disjoint, i.e. no color crosstalk. This spectral crosstalk assumption isn't correct for real sensors, however reconstruction can only be better than what is presented here because spectral crosstalk results in a correlation between colors and doesn't affect the channel bandwidth. We use spatio-temporal statistical image distributions with parameters as we have defined in the past.[12,13,17] The Fourier domain data for an example of the same input data cube for each system is shown in Figure 7 for slow, medium, and fast temporally varying data.

The differences between the Tu and Sony layout are clearly visible for the fast case shown in Figure 7. The s_0 channels are distributed with more spatial bandwidth between them for the Tu case. The Tu s_1, s_2 channels are also offset from the s_0 channels in spatial frequency, reducing channel crosstalk in the temporal frequency direction. The slow case in Figure 7 clearly shows the lower spatial frequency crosstalk of the Tu layout. The Sony layout has 49 channels, while the Tu layout has 33. The Sony layout does have an advantage for the combined s_0 channel at the zero frequency location, especially for high temporal bandwidth data, the Sony layout has less crosstalk along the $\nu = 0$ line than the Tu layout.

4. RESULTS

Performance results are accomplished using PSNR on the 9 parameters for each system. Unmixing is accomplished in the Fourier domain as we have outlined in prior literature.[2,5,12,13,18] Each system uses a 64×64 pixel focal plane array taking 64 frames with identical sampling periods. We compare the various instruments under a fast, medium, and slow spatio-temporal bandwidth scenario as specified in Figure 3. The system performance of the systems was quantified as follows: (1) sets of 8 image blocks of size 64×64×64 were generated from the statistical generation algorithms;[17] (2) a particle swarm algorithm was used to optimize linear Fourier domain filters for 0 center and sideband channels, and for the s_1, s_2 sidebands separately for each system and each bandwidth type, using the mean PSNR[12,13] from the 8 image blocks as the cost function; (3) the mean PSNR for each system was recorded for both systems for each bandwidth type. The Fourier domain filters for the channels have 3 sets of parameters, a set for the $\xi = 0; \eta = 0; \nu = 0$ center channel, a set for the s_0 sidebands in the $\nu = 0$ frequency plane, and a set for the s_1, s_2 sidebands in the $\nu = \pm 0.5$ frequency planes. The preliminary results are shown in Table 1, and we expect the performance differences to increase with a more detailed analysis.

5. CONCLUSION

We have presented some preliminary results on spatio-temporal hybrid color-polarization systems. Given the constraints of a Chun polarization tiling, and a Bayer or quad Bayer color filter tiling with single spectral bandpasses at each pixel, we show here that the solution manufactured by Sony in the new IMX250YMR

Table 1: **Reconstruction PSNR for Various Bandwidth Scenarios**[a]

	Sony	Tu
LSHT	50.5	**50.6**
MSMT	34.0	**34.7**
HSLT	37.5	**38.8**

[a]LSHT = low spatial, high temporal. MSMT = medium spatial, medium temporal. HSLT = high spatial, low temporal. Values are in dB.

isn't as performant as the tiling proposed and prototyped by Tu *et al.*[15] We introduce for the first time a spatio-temporal analysis and design for a hybrid color-polarization micropatterned focal plane array and use our channeled framework to show a clear design choice for the two simplest spatio-temporal hybrid sensor designs. In future work we'll explore panchromatic polarization pixels, and multiband color filters.

ACKNOWLEDGMENTS

This work was funded by the Asian Office of Aerospace Research and Development (FA2386-15-1-4098).

REFERENCES

[1] Vaughn, I. J., Alenin, A. S., and Tyo, J. S., "Bounds on the microanalyzer array assumption," in [*Polarization: Measurement, Analysis, and Remote Sensing XII*], **9853**, 98530W, International Society for Optics and Photonics (2016).

[2] Vaughn, I. J., Alenin, A. S., and Tyo, J. S., "Focal plane filter array engineering I: rectangular lattices," *Optics Express* **25**(10), 11954–11968 (2017).

[3] LaCasse, C. F., Chipman, R. A., and Tyo, J. S., "Band limited data reconstruction in modulated polarimeters," *Opt. Express* **19**, 14976–14989 (Aug 2011).

[4] LeMaster, D. A. and Hirakawa, K., "Improved microgrid arrangement for integrated imaging polarimeters," *Optics letters* **39**(7), 1811–1814 (2014).

[5] Alenin, A. S., Vaughn, I. J., and Tyo, J. S., "Optimal bandwidth micropolarizer arrays," *Optics Letters* **42**(3), 458–461 (2017).

[6] Kudenov, M. W., Pezzaniti, L., Dereniak, E. L., and Gerhart, G. R., "Prismatic imaging polarimeter calibration for the infrared spectral region," *Optics Express* **16**, 13720 – 13737 (2008).

[7] Vaughn, I. J., Rodríguez-Herrera, O. G., Xu, M., and Tyo, J. S., "A portable imaging mueller matrix polarimeter based on a spatio-temporal modulation approach: theory and implementation," *Proc. SPIE* **9613** (2015).

[8] Vaughn, I. J., Rodríguez-Herrera, O. G., Xu, M., and Tyo, J. S., "Bandwidth and crosstalk considerations in a spatio-temporally modulated polarimeter," *Proc. SPIE* **9613** (2015).

[9] Oka, K. and Kato, T., "Spectroscopic polarimetry with a channeled spectrum," *Optics Letters* **24**(21), 1475–1477 (1999).

[10] Wakayama, T., Komaki, K., Vaughn, I. J., Tyo, J. S., Otani, Y., and Yoshizawa, T., "Evaluation of mueller matrix of achromatic axially symmetric wave plate," *SPIE Optical Engineering+ Applications* , 88730P–88730P, International Society for Optics and Photonics (2013).

[11] Vaughn, I., *Bandwidth and Noise in Spatio-temporally Modulated Mueller Matrix Polarimeters*, PhD thesis, College of Optical Sciences, University of Arizona (2016). Appendix A.

[12] Vaughn, I. J., Alenin, A. S., and Tyo, J. S., "A fast stokes polarimeter: preliminary design," in [*Polarization Science and Remote Sensing VIII*], **10407**, 1040702, International Society for Optics and Photonics (2017).

[13] Vaughn, I. J., Alenin, A. S., and Tyo, J. S., "Channeled spatio–temporal stokes polarimeters," *Optics letters* **43**(12), 2768–2771 (2018).

[14] Song, J., Vaughn, I. J., Alenin, A. S., and Tyo, J. S., "Imaging dynamic scenes with a spatio-temporally channeled polarimeter," *Optics Express* **(in press)** (2019).

[15] Tu, X., Spires, O. J., Tian, X., Brock, N., Liang, R., and Pau, S., "Division of amplitude rgb full-stokes camera using micro-polarizer arrays," *Optics Express* **25**(26), 33160–33175 (2017).

[16] Sony, "Sony polarization sensors." `https://www.sony-semicon.co.jp/products_en/IS/sensor5/index.html` (August 2019).

[17] Vaughn, I. J., Alenin, A. S., and Tyo, J. S., "Statistical scene generation for polarimetric imaging systems," *arXiv preprint arXiv:1707.02723* (2017).

[18] Alenin, A. S. and Tyo, J. S., "Generalized channeled polarimetry," *J. Opt. Soc. Am. A* **31**, 1013–1022 (May 2014).